



Contents lists available at ScienceDirect

## Mechatronics

journal homepage: [www.elsevier.com/locate/mechatronics](http://www.elsevier.com/locate/mechatronics)

## Optimal integral force feedback and structured PI tracking control: Application for objective lens positioner

Yik R. Teo<sup>a,\*</sup>, Douglas Russell<sup>b</sup>, Sumeet S. Aphale<sup>b</sup>, Andrew J. Fleming<sup>a</sup>

<sup>a</sup> Precision Mechatronics Lab, School of Electrical Engineering and Computer Science, The University of Newcastle, Callaghan, NSW 2308, Australia

<sup>b</sup> Centre for Applied Dynamics Research, School of Engineering, University of Aberdeen, Aberdeen AB24 3FX, United Kingdom

## ARTICLE INFO

## Article history:

Received 1 July 2013  
Revised 15 April 2014  
Accepted 18 April 2014  
Available online xxx

## Keywords:

Force feedback  
Damping control  
Tracking control  
Nanopositioning

## ABSTRACT

This paper describes a new vibration damping technique based on Integral Force Feedback (IFF). Classical IFF utilizes a force sensor and integral controller to damp the resonance modes of a mechanical system. However, the maximum modal damping depends on the frequency difference between the system's poles and zeros. If the frequency difference is small, the achievable modal damping may be severely limited. The proposed technique allows an arbitrary damping ratio to be achieved by introducing an additional feed-through term to the control system. This results in an extra degree of freedom that allows the position of the zeros to be modified and the maximum modal damping to be increased. The second contribution of this paper is a structured PI tracking controller that is parameterized to cancel the additional pole introduced by integral force feedback. The parameterized controller has only one tuning parameter and does not suffer from reduced phase margin. The proposed techniques are demonstrated on a piezoelectric objective lens positioner. The results show exceptional tracking and damping performance while maintaining insensitivity to changes in resonance frequency. The maximum bandwidth achievable with a commercial PID controller is 26.1 Hz. In contrast, with the proposed damping and tracking controller, the bandwidth is increased to 255 Hz.

© 2014 Elsevier Ltd. All rights reserved.

### 1. Introduction

High-speed precision positioners are widely used in applications such as confocal microscopes [1], scanning probe microscopy [2,3], nanofabrication [4] and electrical characterization of semiconductors [5]. A typical nanopositioning system is illustrated in Fig. 1. One difficulty with nanopositioning systems is the mechanical resonances that arise from the interaction between the platform mass and flexures, mechanical linkages and actuators. As a result, the frequency of the driving signal for instance a triangular reference is commonly limited to 1–10% of the resonance frequency to avoid excitation of the mechanical resonance. In commercial nanopositioning systems the most common type of control is sensor-based feedback control using proportional integral or integral controllers. The benefits of these controllers include robustness to modelling error, simplicity of implementation and reduced piezoelectric non-linearity due to a high loop gain at low frequency. However, the bandwidth of an integral tracking

controller  $C_i(s) = K/s$  is limited by the presence of highly resonant modes. In Refs. [6,7] it was shown that the maximum closed-loop bandwidth is  $2\zeta\omega_n$ , where  $\zeta$  is the damping ratio and  $\omega_n$  is the natural frequency. Since the damping ratio is usually in the order of 0.01, the maximum closed-loop bandwidth is less than 2% of the resonance frequency.

To improve the closed-loop bandwidth of nanopositioning systems, techniques such as notch filters or plant inversion filters can be implemented [8]. Such techniques can provide significantly improved closed-loop bandwidth provided an accurate model of the system is available. Therefore, notch or plant inversion filters are most practical in systems with stable resonance frequencies or where the feedback controller can be continually recalibrated. On the other hand, model-based control such as robust  $\mathcal{H}_\infty$  controllers [9] and LMI based controllers [10] have also been successfully applied to control such systems.

An alternative method to improve the closed-loop response is damping control. Damping controllers have the advantage of being insensitive to variations in resonance frequency. Furthermore, it has been shown that damping controllers provide better external disturbance rejection than inversion-based systems [11]. A number of techniques for damping control have been successfully

\* Corresponding author. Tel.: +61 249217463.

E-mail addresses: [yik.teo@newcastle.edu.au](mailto:yik.teo@newcastle.edu.au) (Y.R. Teo), [r01dr12@abdn.ac.uk](mailto:r01dr12@abdn.ac.uk) (D. Russell), [s.aphale@abdn.ac.uk](mailto:s.aphale@abdn.ac.uk) (S.S. Aphale), [andrew.fleming@newcastle.edu.au](mailto:andrew.fleming@newcastle.edu.au) (A.J. Fleming).

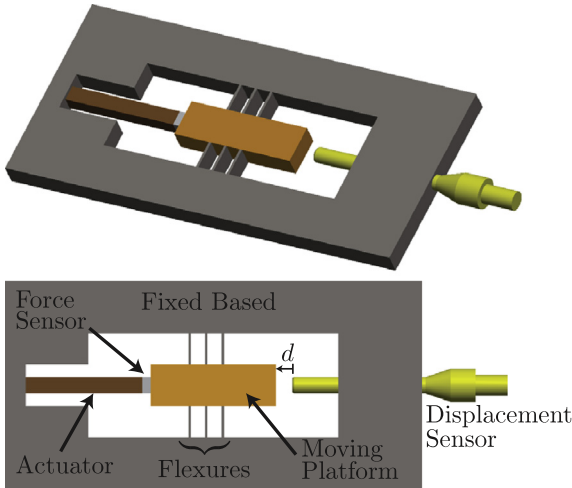


Fig. 1. Single-degree-of freedom positioning stage.

demonstrated in the literature. These include Positive Position Feedback (PPF) [12], polynomial based control [13], acceleration feedback [14], shunt control [15,16], resonant control [17], and Integral Resonance Control (IRC) [18,19]. Among these techniques, PPF controllers, velocity feedback controllers, force feedback controllers, and IRC controllers have been shown to guarantee stability when the plant is strictly negative imaginary [20].

Integral force feedback (IFF) a damping control technique described in Refs. [6,21–25]. The advantages of IFF are the simplicity of the controller, guaranteed stability and excellent performance robustness. Furthermore, IFF can also be implemented using an analog filter. However, one of the limitations of IFF is that the maximum modal damping depends on the frequency difference between the system's poles and zeros. If the frequency difference is small, the achievable modal damping may be severely limited. Furthermore, when the IFF system is enclosed in a tracking loop, the closed-loop performance is limited by an additional pole introduced by the integral force feedback controller.

In this work, we proposed a technique that allows an arbitrary damping ratio to be achieved by introducing an additional feed-through term to the control system. This allows the position of the zeros to be modified, hence, increasing the maximum modal damping. Furthermore, we identified the additional pole that is introduced by the integral force feedback controller and compensate it by parameterising the tracking controller with a zero that cancels the additional pole.

The remainder of the paper is organized as follows. In Section 2, the modelling of a single-degree-of-freedom positioning system is shown. Section 3 compares the proposed damping control technique with classical integral force feedback control. The tracking controller designs are discussed in Section 4. A simulation example is shown Section 5 follow by the experimental result on a commercial objective lens positioner in Section 6.

## 2. Modelling a nanopositioning system

The single-degree-of-freedom positioner illustrated in Fig. 2 can be represented by a second-order mechanical system. The equation of motion for this system is

$$M_p \ddot{d} + c_f \dot{d} + (K_a + k_f)d = F_a, \quad (1)$$

where  $M_p$  is the mass of the platform and the stiffness and damping coefficient of the flexures are denoted by  $k_f$  and  $c_f$  respectively. The force applied by the actuator is  $F_a$  and the actuator stiffness is  $K_a$ . A

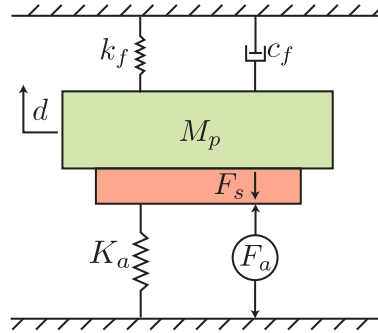


Fig. 2. Mechanical diagram of a single-degree-of freedom positioner where  $F_s$  is the measured force acting between the actuator and the mass of the platform in the vertical direction.

force sensor is collocated with the actuator and measures the load force,  $F_s$ .

The configuration of the system is such that the actuator and flexure appear mechanically in parallel, hence, the stiffness coefficients can be grouped together,  $k = K_a + k_f$  which simplifies the equation of motion (1) to

$$M_p \ddot{d} + c_f \dot{d} + k = F_a. \quad (2)$$

The transfer function from actuator force,  $F_a$ , to the displacement of the platform,  $d$  is

$$G_{dF_a}(s) = \frac{d}{F_a} = \frac{1}{M_p s^2 + c_f s + k}. \quad (3)$$

The sensor force,  $F_s$ , can be written as

$$\begin{aligned} F_s &= F_a - dK_a, \\ &= F_a - K_a F_a G_{dF_a}(s), \\ &= F_a (1 - K_a G_{dF_a}(s)). \end{aligned} \quad (4)$$

The transfer function between the applied force,  $F_a$ , and measured force,  $F_s$ , is found by rearranging (4).

$$G_{F_s F_a}(s) = \frac{F_s}{F_a} = 1 - K_a G_{dF_a}(s). \quad (5)$$

The force developed by the actuator,  $F_a$ , is

$$F_a = K_a \delta \quad (6)$$

where  $\delta$  is the unconstrained piezo expansion.

Substituting (6) into (5), we obtain the transfer function from the unconstrained piezo expansion  $\delta$  to the force of the sensor  $F_s$

$$G_{F_s \delta} = \frac{F_s}{\delta} = K_a \frac{F_s}{F_a} = K_a (1 - K_a G_{dF_a}(s)). \quad (7)$$

A valid assumption is that the effect of the damping in the flexure,  $c_f$ , is small and thus negligible. The frequency of the open-loop poles  $\omega_1$  and zeros  $z_1$  of (5) are

$$\omega_1 = \sqrt{\frac{k}{M_p}} = \sqrt{\frac{K_a + k_f}{M_p}} \quad z_1 = \sqrt{\frac{k_f}{M_p}}. \quad (8)$$

## 3. Damping control

Integral Force Feedback (IFF) is a popular method for damping control, as described in Refs. [6,21–25]. This technique utilizes a force sensor and integral controller to directly augment the damping of a mechanical system. The major advantages of IFF is the simplicity of the controller, guaranteed stability, excellent performance robustness, and the ability to damp a large number

of resonance modes with a first order controller. Moreover, a piezoelectric force sensor has significantly lower noise density as compared to inductive or resistive strain sensors [26].

### 3.1. Classical integral force feedback

The technique of Classical Integral Force Feedback (CIFF) has been widely applied for augmenting the damping of flexible structures. The feedback law is simple to implement and, under common circumstances, provides excellent damping performance with guaranteed stability.

The open loop transfer function between the unconstrained piezo expansion  $\delta$  to the sensor force  $F_s$  is adapted from Ref. [22]

$$G_{F_s, \delta}(s) = \frac{F_s}{\delta} = K_a \left\{ 1 - \sum_{i=1}^n \frac{v_i}{1 + s^2/\omega_i^2} \right\}, \quad (9)$$

where the sum extends to all the modes,  $\omega_i$  is the natural frequency of the system and  $v_i$  is the fraction of modal strain energy for the  $i$ th mode. The corresponding zeros of each mode is given as  $z_i^2 = \omega_i^2(1 - v_i)$  [22].

For the positioning application the first resonance mode is of significant interest, this reduce (9) to a second order system (7). The feedback diagram of an IFF damping controller is shown in Fig. 3(a). The frequency response of  $G_{F_s, F_a}$  is shown in Fig. 4. A key observation of the system  $G_{F_s, F_a}$  is that its phase response lies between  $0^\circ$  and  $180^\circ$ . This is a general feature of flexible structures with inputs and outputs proportional to applied and measured forces. A unique property of such systems is that integral control can be directly applied to achieve damping, i.e.

$$C_{d1}(s) = \frac{K_{d1}}{K_a s}, \quad (10)$$

where  $K_{d1}$  is the damping control gain. As the integral controller has a constant phase lag of  $90^\circ$ , the loop-gain phase lies between  $-90$  and  $90^\circ$ . That is, the closed-loop system has an infinite gain margin and phase margin of  $90^\circ$ . Simplicity and robustness are two outstanding properties of systems with CIFF.

A solution for the optimal feedback gain has already been derived in [22]. These results can be directly adapted for the system considered in this study. The method makes the valid assumption that system damping coefficients are small and can be

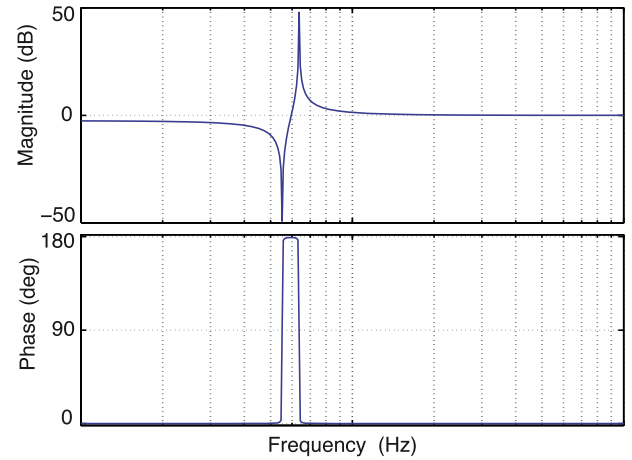


Fig. 4. Typical frequency response of  $G_{F_s, F_a}(s)$ .

neglected. With these assumptions, the maximum modal damping is [22]

$$\zeta_i^{max} = \frac{\omega_i - z_i}{2z_i}, \quad (11)$$

and is achieved for

$$K_{d1} = \omega_i \sqrt{\frac{\omega_i}{z_i}}. \quad (12)$$

The root locus plot corresponding to CIFF is shown in Fig. 5(a). Note that a key characteristic of this system is that the position of the poles and zeros alternates. The main limitation of the classical method is that the maximum modal damping (11) depends on the distance between the system poles  $\omega_i$  and modal zeros  $z_i$ . If the distance between the pole and zero is small, the maximum modal damping achievable with CIFF is reduced. This means that some systems can be critically damped using CIFF while other systems exhibit insufficient damping.

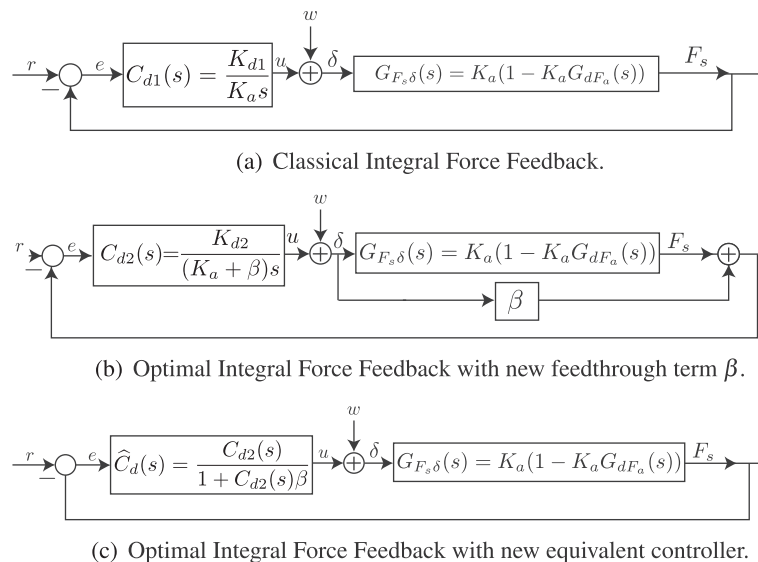


Fig. 3. Damping control: Integral force feedback block diagrams.

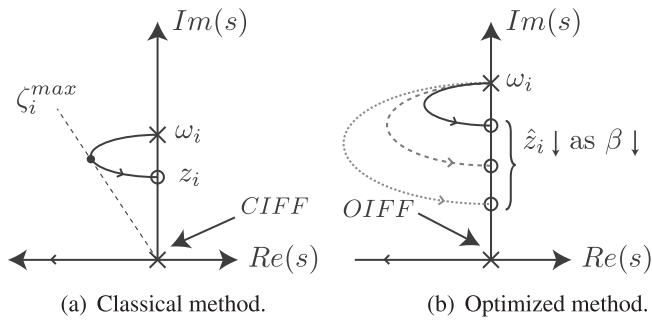


Fig. 5. Damping control: Typical root locus plots.

3.2. Optimal integral force feedback

Here, we discuss an extension to the classical technique of integral force feedback that allows an arbitrary damping ratio to be achieved for any system. A new feed-through term  $\beta$  is introduced into the system as shown in Fig. 3(b). The location of the modal zeros is given as

$$\hat{z}_i(\beta) = \sqrt{\omega_i^2 \left( 1 - \frac{K_a}{K_a + \beta} \frac{K_a}{k} \right)}. \quad (13)$$

This results in an extra degree of freedom that allows the position of the zeros to be modified. As  $\beta$  decreases, the zeros of the system will move closer to the real axis, under the condition that  $K_a(v_i - 1) < \beta < 0$  is satisfied. The new maximum damping ratio of the system is given as

$$\hat{\zeta}_i^{\max} = \frac{\omega_i - \hat{z}_i(\beta)}{2\hat{z}_i(\beta)}, \quad (14)$$

The controller is given as

$$C_{d2}(s) = \frac{K_{d2}}{(K_a + \beta)s}. \quad (15)$$

The corresponding optimal gain is given as

$$K_{d2} = \omega_i \sqrt{\frac{\omega_i}{\hat{z}_i(\beta)}}. \quad (16)$$

Given a desired damping ratio  $\zeta_d < 1$ , the expression for  $\beta$  is found by replacing (13) into (14) and rearranging the equation as

$$\beta = -K_a + \frac{K_a v_i (2\zeta_d + 1)^2}{4\zeta_d (1 + \zeta_d)}, \quad (17)$$

where  $v_i = K_a/k$  for the nanopositioning system in Section 2. The typical root locus plot corresponding to OIFF is given in Fig. 5(b). Note that the zero location changes with respect to  $\beta$ . The equivalent controller  $\hat{C}_d(s)$  can be written as

$$\hat{C}_d(s) = \frac{C_{d2}(s)}{1 + C_{d2}(s)\beta}, \quad (18)$$

as shown in Fig. 3(c). The modification amounts to replacing the integral controller with a first-order low-pass filter. Although the

additional complexity is negligible, the damping performance is significantly improved. This result allows integral force feedback control to be applied to systems that were not previously suited.

4. Tracking control

4.1. Integral control with displacement feedback

The most straightforward technique for achieving displacement tracking is to simply enclose the system in an integral feedback loop, as depicted in Fig. 6. The tracking controller  $C_{t1}(s)$  is simply

$$C_{t1}(s) = \frac{K_{t1}}{s}. \quad (19)$$

In this strategy, the displacement,  $d$ , must be obtained with a physical displacement sensor such as a capacitive, inductive, or optical sensor [26]. However, from the pole-zero map shown in Fig. 7, the damped system contains a pair of resonance poles, plus an additional real axis pole due to OIFF. The additional pole unnecessarily increases the system order and reduces the achievable tracking bandwidth due to low-phase margin.

The characteristic equation of the closed-loop transfer function is given by the numerator of

$$1 + \frac{K_{t1}K_{d1}}{\gamma_4 s^4 + \gamma_3 s^3 + \gamma_2 s^2 + \gamma_1 s^1}, \quad (20)$$

where

$$\gamma_4 = K_a M_p + M_p \beta, \quad (21)$$

$$\gamma_3 = c_f K_a + K_a K_{d1} M_p + c_f \beta + K_{d1} M_p \beta, \quad (22)$$

$$\gamma_2 = k K_a + c_f K_a K_{d1} + k \beta + c_f K_{d1} \beta, \quad (23)$$

$$\gamma_1 = k K_a K_{d1} - K_a^2 K_{d1} + k K_{d1} \beta. \quad (24)$$

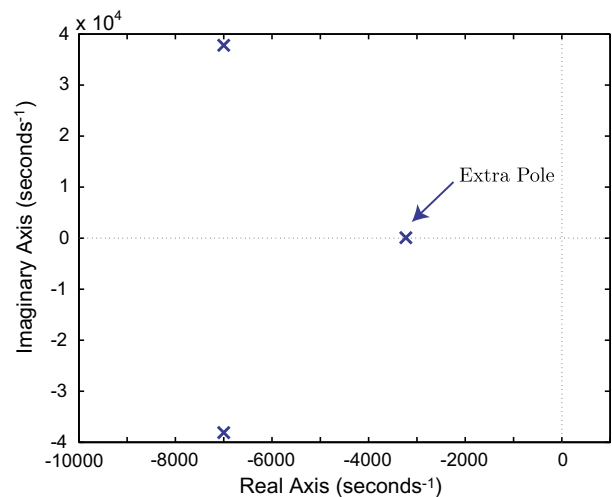


Fig. 7. Pole-zero map of the damping loop.

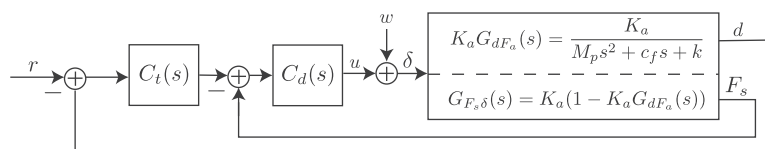


Fig. 6. Tracking loop.

**Proposition 1.** Let  $K_{d1}$  and  $K_{t1}$  be the OIFF damping and integral tracking gain respectively. For a closed-loop system as implemented in Fig. 6 to be stable, the gains must obey the following inequality:

$$K_{d1}K_{t1} < \frac{(K_a^2(-K_a^2 + k(K_a + \beta)))}{(M_p(K_a + \beta))}. \quad (25)$$

**Proof.** In order to check the stability of the closed-loop transfer function, the zeros/numerator of (20) should be evaluated. The system is stable if all the zeros have negative real parts. Assuming that damping in the system is negligible, all necessary and sufficient conditions for stability are met if (1) all the coefficients of (20) are positive and (2) all the elements of the first column of the Routh-Hurwitz table are positive. The condition of stability is given as

$$K_{d1}^3 K_{t1} M_p (K_a + \beta) (K_a M_p + M_p \beta) + K_{d1}^2 M_p (K_a + \beta) (K_a^4 - k K_a^2 (K_a + \beta)) < 0. \quad (26)$$

Rearranging (26) for  $K_{t1}K_{d1}$  results in the expression (25).  $\square$

#### 4.2. Structured PI control with displacement feedback

The location of the additional pole can be found by examining the characteristic Eq. (20) of the damped system. For the system under consideration, the roots of the characteristic equation contain a complex pair and a pole on the real axis as shown before.

To eliminate the additional pole from the tracking loop, the controller can be parameterised so that it contains a zero at the same frequency. A controller that achieves this is

$$C_{t2}(s) = \frac{K_{t2}(s + p)}{sp}, \quad (27)$$

where  $p$  is the location of the additional pole identified by finding the roots of (20) using Cardano's method [27],

$$p = -(A + B - a/3),$$

$$a = K_{d2} + \frac{c_f}{M_p},$$

$$b = \frac{k + c_f K_{d2}}{M_p},$$

$$c = \frac{K_{d2}(-K_a^2 + k(K_a + \beta))}{M_p(K_a + \beta)},$$

$$Q = \frac{a^2 - 3b}{9}, \quad R = \frac{2a^3 - 9ab + 27c}{54},$$

$$A = -\sqrt[3]{R + \sqrt{R^2 - Q^3}}, \quad B = Q/A.$$

The integral gain is chosen in the normal way to provide the desired stability margins. The form of this controller is identical to a PI controller except that the zero location is fixed. This is advantageous since the controller has only one free tuning parameter.

### 5. Example system

Here, we examine a single degree of freedom positioner based on the mechanical diagram shown in Fig. 2 with mass  $M_p = 250$  g, flexure stiffness  $k_f = 300$  N/ $\mu$ m, actuator stiffness  $K_a = 100$  N/ $\mu$ m and flexure damping  $c_f = 10$  N/m  $s^{-1}$ . The frequency of the open-loop poles and zeros of the system are

$$\omega_1 = 6.37 \text{ kHz} \quad z_1 = 5.5 \text{ kHz}. \quad (28)$$

The optimal gain and maximum damping ratio for the example system using CIFF is  $K_{d1} = 4.3 \times 10^4$  and  $\zeta_1^{max} = 0.077$ . The numerically

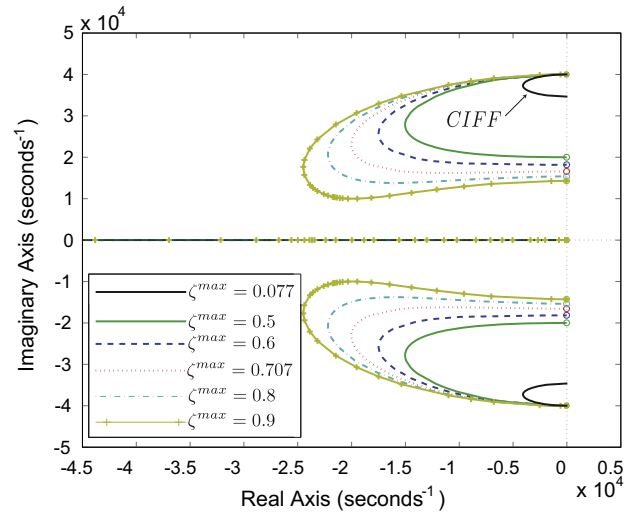


Fig. 8. Example system: Root locus comparison between CIFF and OIFF.

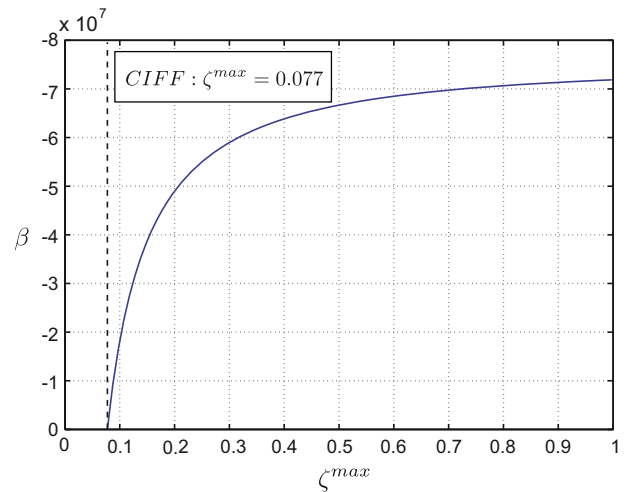


Fig. 9. Example system: The relationship between  $\beta$  and  $\zeta$  for OIFF.

obtained optimal gain is  $4.57 \times 10^4$  and the damping ratio is 0.077. These values are obtained from the root-locus plot shown in Fig. 8 and correlate closely with the predicted values which supports the accuracy of the assumptions made in deriving the optimal gain. With OIFF, the relationship between  $\beta$  and  $\zeta$  is described in (17) and plotted in Fig. 9. The maximum modal damping with CIFF is 0.077; however, with OIFF, the maximum modal damping can be varied from 0.077 to 1 at different values of  $\beta$ .

The root locus of the system is shown in Fig. 8. The optimal feedback gain, maximum damping ratio and corresponding value of  $\beta$  is given in Table 1. These values can be validated by the numerical root-locus plot in Fig. 8 and are summarized in Table 1.

If a disturbance,  $w$ , is added into the system. The transfer function from the disturbance,  $w$ , to the sensor force,  $F_s$ , is

$$G_{F_s w}(s) = \frac{F_s}{w} = \frac{G_{F_s \delta}}{1 + C_d G_{F_s \delta}}, \quad (29)$$

where  $C_d = C_{d1}$  for CIFF and  $C_d = \hat{C}_d$  for OIFF. The simulated open-loop and closed-loop frequency responses of (29) are plotted in Fig. 10 for both CIFF and OIFF. The transfer function from the disturbance  $w$  to the displacement of the platform  $d$  are given as

$$G_{dw}(s) = \frac{d}{w} = \frac{K_a G_{d F_a}}{1 + C_d G_{F_s \delta}}. \quad (30)$$

**Table 1**  
Comparison between analytic and numerically obtained damping ratio  $\zeta^{max}$  and feedback gain  $K_{d2}$  for the example system.

$\beta$	Analytic		Numerical	
	$\zeta^{max}$	$K_{d2}$	$\zeta^{max}$	$K_{d2}$
$-6.67 \times 10^7$	0.500	$5.65 \times 10^4$	0.501	$5.57 \times 10^4$
$-6.98 \times 10^7$	0.707	$6.21 \times 10^4$	0.708	$6.23 \times 10^4$
$-7.13 \times 10^7$	0.900	$6.69 \times 10^4$	0.902	$6.70 \times 10^4$

The simulated open-loop and closed-loop frequency responses of (30) for both cases are shown in Fig. 11. For the OIFF case, the closed-loop transfer function measured from the reference,  $r$ , to the sensor force,  $F_s$ , is

$$G_{F_s r}(s) = \frac{F_s}{r} = \frac{C_d G_{F_s \delta}}{1 + C_d G_{F_s \delta}}, \quad (31)$$

when  $s = 0$

$$G_{F_s r}(0) = \frac{C_d G_{F_s \delta}(0)}{1 + C_d G_{F_s \delta}(0)} = \frac{G_{F_s \delta}(0)}{G_{F_s \delta}(0) + \beta}. \quad (32)$$

This shows that the DC gain of the closed-loop increases as  $\beta$  is decreased. Recall that the maximum damping ratio of the closed-loop system increases as  $\beta$  is decreased.

In addition, the effect of control action with respect to input disturbance is examined. The transfer function between the input disturbance  $w$  to the control action  $u$  is

$$G_{uw}(s) = \frac{u}{w} = \frac{C_d G_{F_s \delta}}{-1 - C_d G_{F_s \delta}}. \quad (33)$$

The frequency response of this transfer function is shown in Fig. 12. The sensitivity of the control action toward input disturbance increases as the desired damping ratio is increased.

We now examine the performance of the tracking controllers. The example system is damped using OIFF with a desired damping ratio of 0.707. With the basic integral tracking control, the closed-loop bandwidth of the system is 400 Hz with a gain margin of 20 dB. As expected, the closed-loop bandwidth is limited by low-phase margin. The corresponding damping and tracking gain are  $6.21 \times 10^4$  and  $4.0 \times 10^{10}$ . The product of the two gains satisfies the stability condition given in (25). However, with the structured PI tracking controller, the closed-loop bandwidth of the system is increased to 1200 Hz with a phase-margin of 60°. This shows an

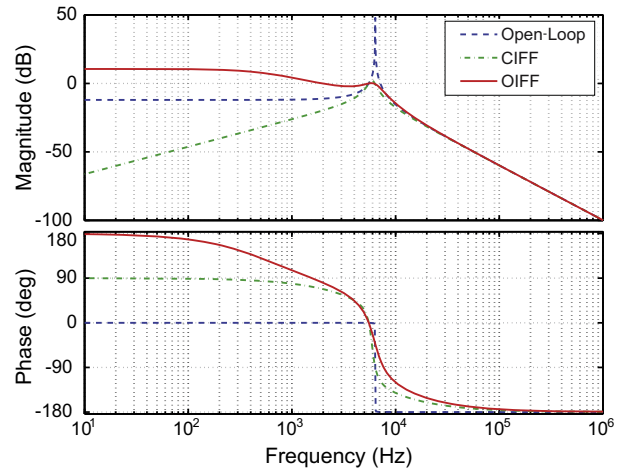


**Fig. 11.** Example system: Frequency response from the input disturbance  $w$  to the displacement of the platform  $d$ .

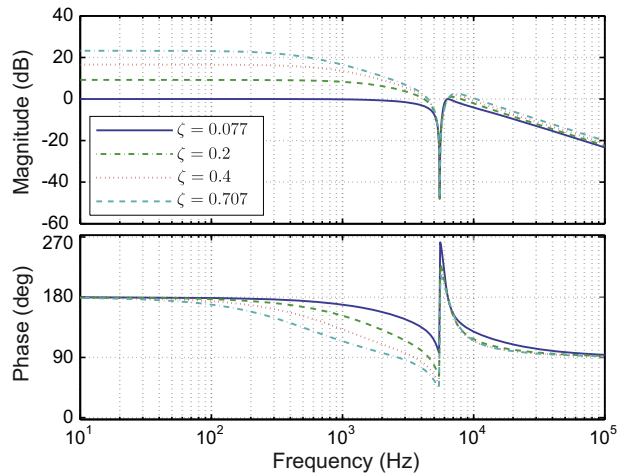


**Fig. 12.** Example system: Frequency response from the input disturbance  $w$  to the control action  $u$  as  $\beta$  is increased.

improvement of threefold just by cancelling an additional real pole induced by the inner damping loop. Fig. 13 shows the closed-loop frequency response of the system using the two tracking control architecture discussed previously.

To examine the constant velocity tracking performance, a triangular waveform was applied as a reference with a frequency of 200 Hz. Fig. 14(a) shows the displacement of the system. The tracking error is plotted in Fig. 14(b). The optimal force feedback controller can be observed to heavily reduce the tracking error.

5.1. Effect of higher order modes

So far, only a single degree of freedom system has been considered. Although this is appropriate for modelling the first resonance mode, it does not capture the higher order modes that occur in distributed mechanical systems. However, the higher order modes do not disturb the zero-pole ordering of the transfer function from the applied actuator voltage to the measured force. To illustrate this concept, we augment the open-loop system with an additional second-order system at five times the resonance frequency of the first mode. Fig. 15 shows the closed-loop frequency responses of the system. Note that the second mode does not affect the performance of the system.

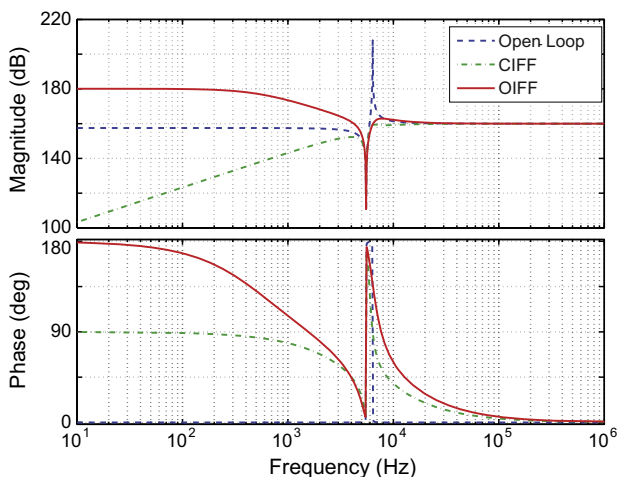


**Fig. 10.** Example system: Frequency response from the input disturbance  $w$  to the sensor force  $F_s$ .

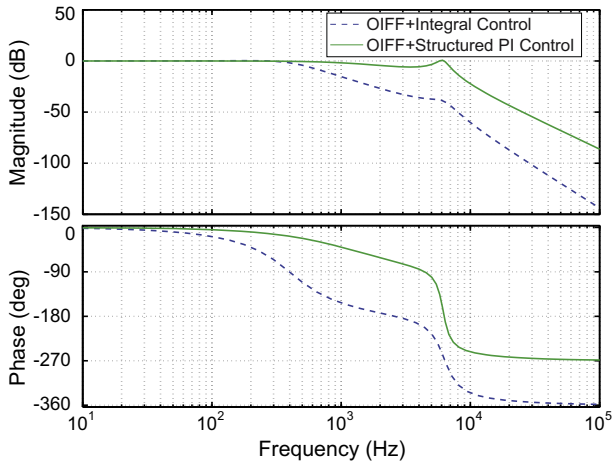
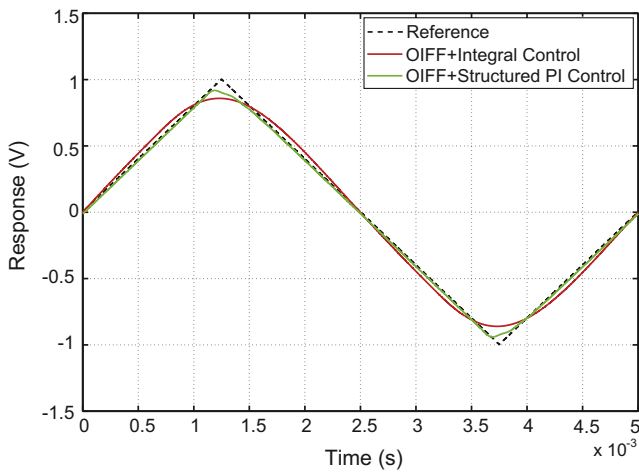
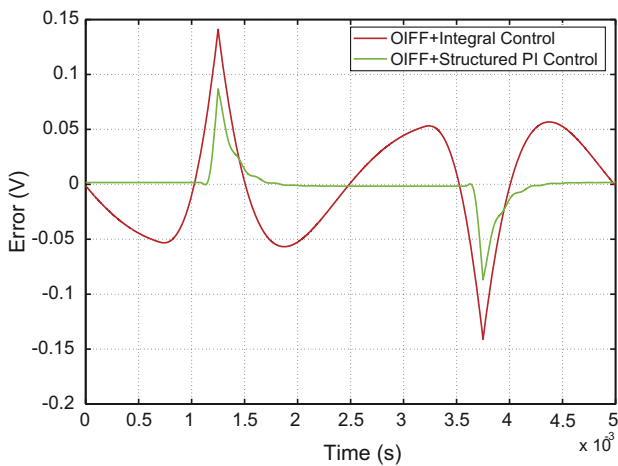


Fig. 13. Example system: Closed-loop frequency responses from the reference  $r$  to the displacement of the platform  $d$  of the system.



(a) Position



(b) Error

Fig. 14. Example system: Constant velocity tracking with triangular wave.

The transfer function of a generalized mechanical system with a discrete piezoelectric transducer and collocated force sensor is guaranteed to exhibit zero-pole ordering as shown in [22]. That is, the transfer function  $G_{F_s F_a}$  will always exhibit zero-pole ordering. As the zero-pole ordering of the system is guaranteed, it

follows that the controller discussed in the previous section will also guarantee the stability of systems with multiple modes.

### 6. Application to objective lens positioner

The experiment was conducted on a Queensgate OSM-Z-100B objective lens positioner with 3 different objective loads as shown in Fig. 16. This single-axis lens positioner has a range of 100  $\mu\text{m}$  and a static stiffness of 1.5 N/m. The inner loop damping controller is implemented using analog electronics. The outer tracking loop is implemented using a Queensgate NPS4110 controller. The block diagram of the experimental setup is shown in Fig. 17.

By referring to set-up in Fig. 17, the open-loop frequency response of the positioner with 100 $\times$  objective was measured from the voltage amplifier input  $u_2$  which is proportional to the internal actuator force,  $F_a$ , to the force sensor,  $F_s$ , and position sensor output,  $d$ , with an excitation of 100 mV<sub>pp</sub> random noise signal. The open-loop frequency responses are shown in Fig. 18 which exhibits a resonance frequency at around 383 Hz. The first two modes are relatively close in frequency. The system can be approximated by a second-order transfer function given as

$$G_{F_s F_a}(s) = \frac{2.141s^2 + 736.4s + 6.072 \times 10^6}{s^2 + 214s + 5.606 \times 10^6} \quad (34)$$

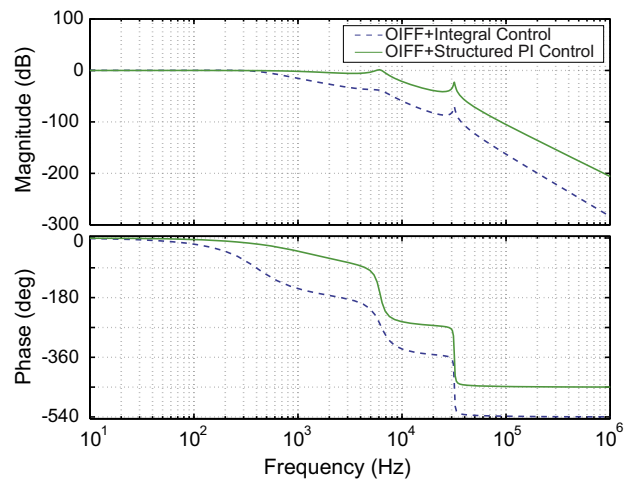


Fig. 15. Example system: Closed-loop frequency responses from the reference  $r$  to the displacement of the platform  $d$  of the system with higher order model.



Fig. 16. Queensgate OSM-Z-100B objective lens positioner (Left) and Olympus 4 $\times$ , 40 $\times$  and 100 $\times$  objective lens (Right).

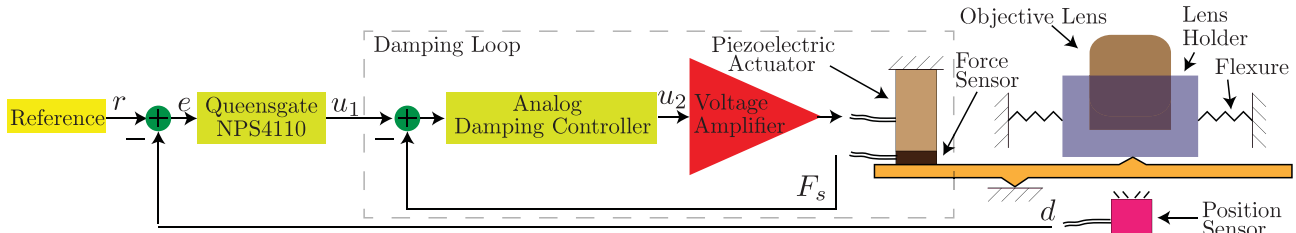
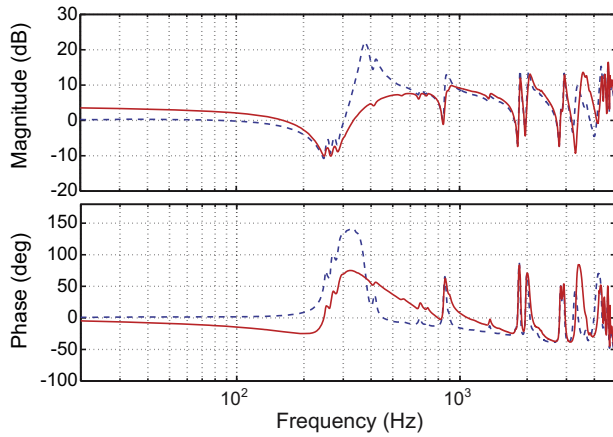
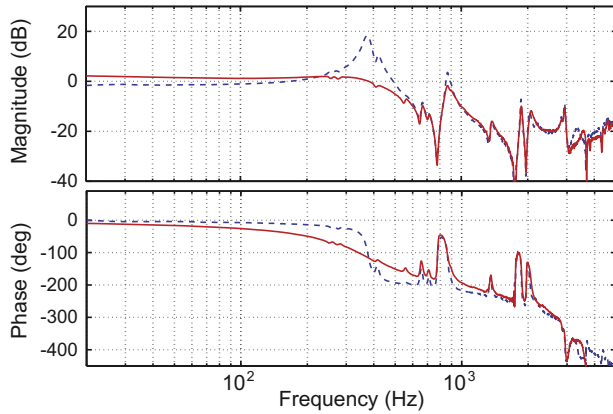


Fig. 17. Block diagram of the experimental setup.



(a) Open-loop (dashed line) frequency response measured from  $u_2$  to the output of the sensor force and closed-loop (solid line) frequency response measured from  $u_1$  to the output of the sensor force.



(b) Open-loop (dashed line) frequency response measured from  $u_2$  to the output of the position sensor and closed-loop (solid line) frequency response measured from  $u_1$  to the output of the position sensor.

Fig. 18. Experimental results: Open-loop and closed-loop frequency responses using CIFF and OIFF.

6.1. Damping controller design

The optimal gain and maximum damping ratio of system (34) using CIFF are  $K_{d1} = 1500$  and  $\zeta_1^{max} = 0.3$ . These values can also be obtained numerically from the root locus plot in Fig. 19. The numerically found optimal gain is 1700 and the corresponding damping ratio is 0.33. Fig. 19 also includes the root locus plots of the system using OIFF with different feed-through terms  $\beta$ . The relationship between  $\beta$  and  $\zeta^{max}$  (shown in Fig. 20) was numerically obtained from the root locus plot and summarized in Table 2. The maximum damping ratio is increased from 0.33 (CIFF) to 0.85 by just adjusting the value of  $\beta$ . Fig. 18 includes the closed-loop

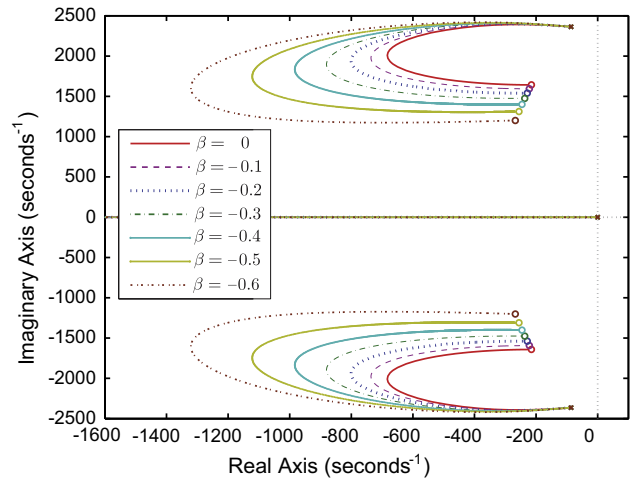


Fig. 19. Experimental results: Root locus using OIFF.

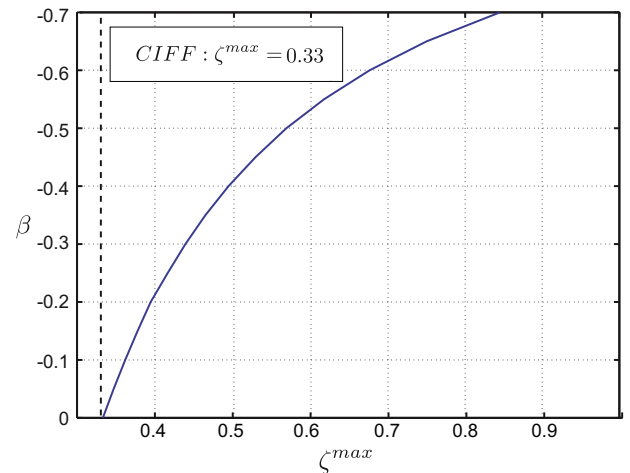


Fig. 20. Experimental results: Relationship between  $\zeta^{max}$  and  $\beta$  using OIFF.

frequency responses of the system using OIFF with  $\beta = -0.6$ . The closed-loop frequency responses are measured using the same procedure as the open-loop responses. The closed-loop response shows that the first and second resonance modes have been effectively eliminated. The higher frequency modes have also been damped by up to 5 dB.

6.2. Tracking control design

The performance of the commercial PID controller was tuned experimentally to minimized the settling time due to a step input reference. The implemented PID controller has the following structure

**Table 2**  
Experimental results: Numerically obtained data for OIFF.

$\beta$	$\zeta_1^{max}$	$K_{d2}$	$\beta$	$\zeta_1^{max}$	$K_{d2}$
0.0	0.33	1700	-0.4	0.49	2350
-0.1	0.36	1840	-0.5	0.57	2500
-0.2	0.39	2060	-0.6	0.68	2840
-0.3	0.44	2160	-0.7	0.85	3300

$$C_r(s) = k_p + \frac{k_i}{s} + \frac{k_d s}{\tau_d s + 1}, \quad (35)$$

where  $k_p = 0.01$ ,  $k_i = 2000$ ,  $k_d = 1 \times 10^{-6}$  and  $\tau_d = 1.25 \times 10^{-7}$ . The derivative component is an approximation that facilitates practical implementation. The approximation acts as a derivative at low frequency, while reducing the gain at high frequency with an additional pole [28]. The term  $\tau_d$  limits the gain, hence, the high-frequency signal is amplified at most by a factor of  $k_d/\tau_d = 8$ .

The structured PI controller is

$$C_r(s) = \frac{700(s + 2914)}{2914s}, \quad (36)$$

where  $s = -2914$  is the location of the additional pole. The only tuning parameter here is  $K_i$  which was tuned to provide acceptable stability margins. The loop return ratio plot of the controllers are shown in Fig. 21. The gain and phase margin of the system with commercial PID control is 3.2 dB and 86° respectively. The gain and phase margin of the system with Optimal Integral Force Feedback and Structured PI control is 17.3 dB and 75° respectively.

The closed-loop frequency responses of the standard commercial controller and the proposed controller are plotted in Fig. 22. The achievable tracking bandwidth of the commercial PID controller is 26.1 Hz compared to 255 Hz with the proposed controller.

### 6.3. Sensitivity to variations in resonance frequency

The force feedback loop was initially tuned for the 100× objective which has a nominal mass of 88.8 g. In order to show the insensitivity to variation in resonance frequency, other objectives were considered without retuning the tracking loop. The objectives are 4× objective (47.8 g) and a modified 40× objective (163.3 g). The variations in resonance frequency and performance are summarized in Table 3. The open-loop and force feedback response of the stage with different loads are plotted in Figs. 23 and 24. It

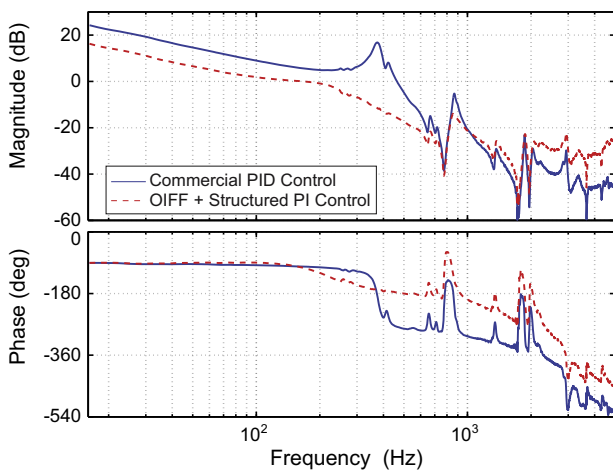


**Fig. 21.** Experimental result: Comparison between the loop return ratio plots of the system with a commercial PID controller (solid line) and Optimal Integral Force Feedback and Structured PI Control (dashed line).

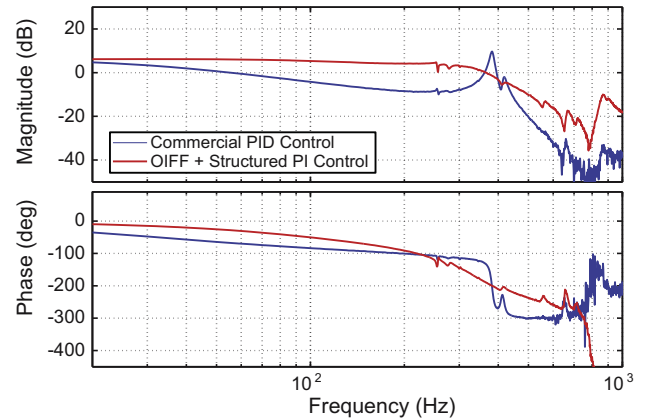


**Fig. 22.** Experimental result: Closed-loop frequency response of the tracking loop measured from  $r$  to the position sensor output  $d$ , scaled to  $\mu/V$ .

**Table 3**  
Experimental results: Influence of objective mass on performance.

	4×	100×	40× + mass
Mass	47.8 g	88.8 g	163.3 g
Resonance Freq.	412 Hz	378 Hz	264 Hz
Force Feedback BW	500 Hz	398 Hz	326 Hz
Tracking BW (PID)	31.6 Hz	26.1 Hz	21.5 Hz
Tracking BW (OIFF)	167 Hz	255 Hz	212 Hz

can be observed that the tuning of the force feedback loop is not sensitive to changes in resonance frequency. The tracking controller frequency responses with, and without force feedback are plotted in Figs. 25 and 26. As expected from the results in Fig. 24, the only significant change in the force feedback response is the bandwidth, which is proportional to the resonance frequency.

### 6.4. Constant velocity tracking and step response

To examine the constant velocity tracking performance, a 80  $\mu\text{m}$  sawtooth waveform was applied as a reference with a frequency of 3 Hz and at 95% duty cycle. Fig. 27(a) shows the displacement of the system. The tracking error is plotted in Fig. 27(b). The optimal force feedback controller can be observed to reduce the tracking error by up to 65%.

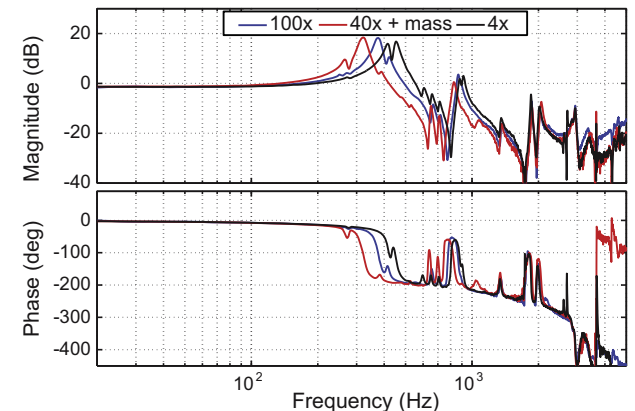


**Fig. 23.** Experimental results: Open-loop frequency response measured from  $u_2$  to the output of the position sensor output  $d$ , scaled to  $\mu/V$  with different objectives.

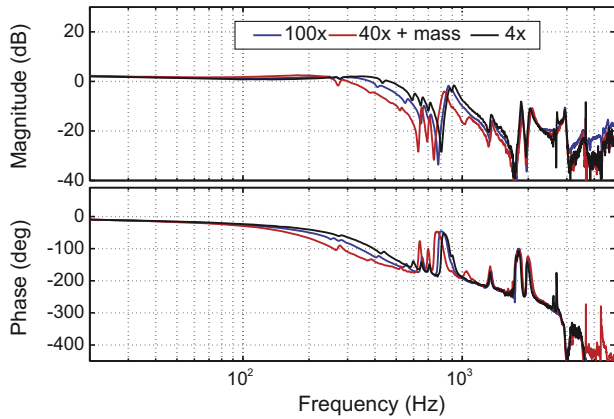


**Fig. 24.** Experimental results: Closed-loop frequency response of the damping loop measured from  $u_1$  to the output of the position sensor output  $d$ , scaled to  $\mu/V$  with different objectives.

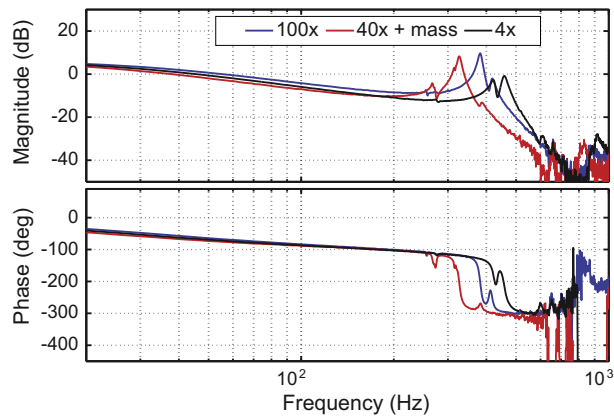


**Fig. 25.** Experimental results: Closed-loop frequency response of the tracking loop measured from  $r$  to the output of the position sensor output  $d$ , scaled to  $\mu/V$ , with a commercial PID controller.

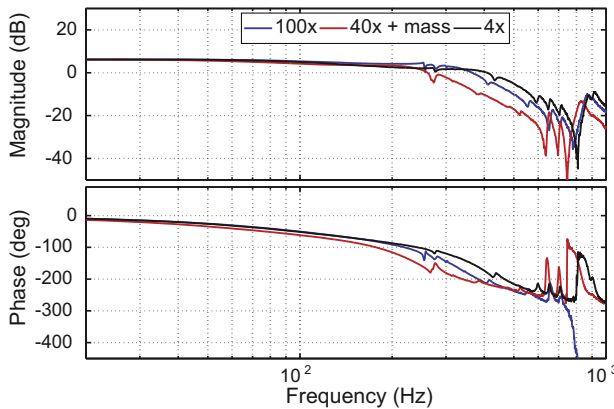
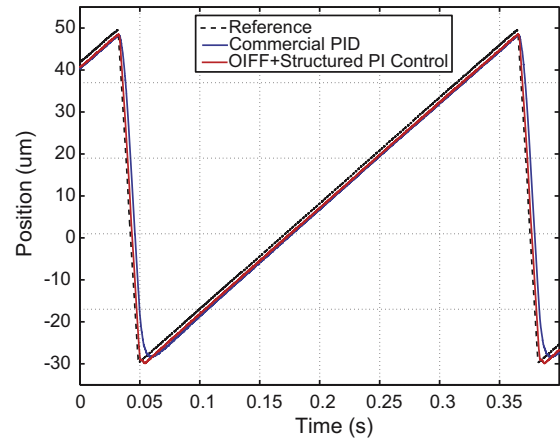
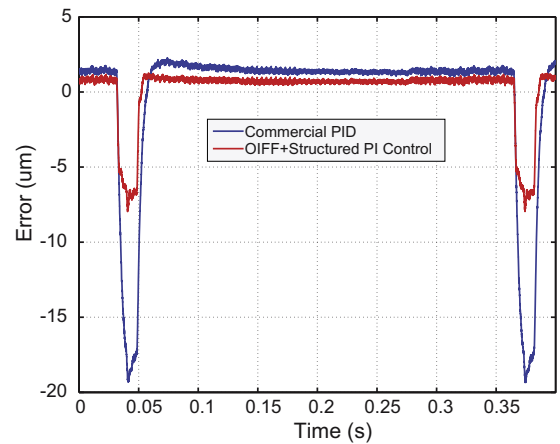


**Fig. 26.** Experimental results: Closed-loop frequency response of the tracking loop measured from  $r$  to the position sensor  $d$ , scaled to  $\mu/V$ , with Optimal Integral Force Feedback and Structured PI control.

The step responses for different objective masses are also plotted in Fig. 28. The heavier objective requires a proportionally longer settling time. The settling time of the system with the proposed damping and tracking controller is greatly improved compared to the standard PID controller.



(a) Position



(b) Error

**Fig. 27.** Experimental results: Constant velocity tracking of a  $80\ \mu\text{m}$  sawtooth waveform with a frequency of 3 Hz and at 95% duty cycle.

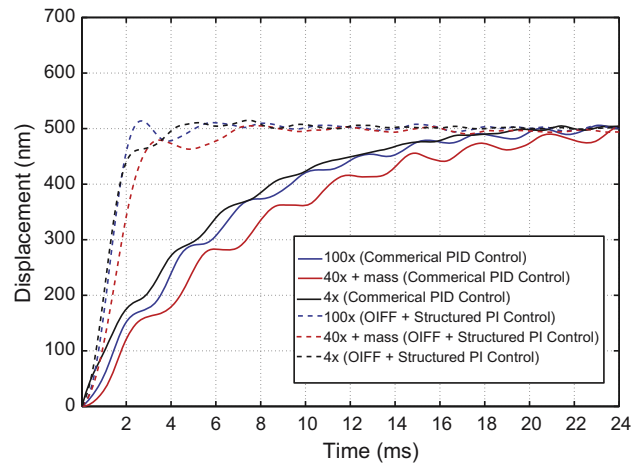


**Fig. 28.** Experimental results: Closed-loop step response comparison between different objectives and controllers. The step reference is  $500\ \text{nm}$ .

## 7. Conclusions

The maximum damping achievable with classical integral force feedback control is limited by the frequency difference between the systems poles and zeros. This paper describes a novel improvement that allows an arbitrary damping ratio to be achieved for any

system by introducing an additional feed-through term. For systems with closely spaced poles and zeros, the damping performance may be significantly improved.

The second contribution is a structured PI controller for tracking loop of systems with force feedback. The proposed tracking controller is parameterized so that it contains a zero that cancel the additional pole due introduced by the damping controller. This approach improves the system phase margin and closed-loop servo bandwidth.

The proposed techniques are demonstrated on an objective lens positioning system. With a commercial PID controller, the maximum tracking bandwidth is 26.1 Hz. However, with the proposed tracking and damping controller, the tracking bandwidth is increased to 255 Hz.

## References

- [1] Semwogerere D, Weeks ER. Confocal microscopy. In: Wnek G, Bowlin G, editors. *Encyclopedia of biomaterials and biomedical engineering*. New York: Taylor and Francis; 2004.
- [2] Salapaka SM, Salapaka MV. Scanning probe microscopy. *IEEE Control Syst* 2008;28(2):65–83.
- [3] Leang KK, Fleming AJ. High-speed serial-kinematic AFM scanner: design and drive considerations. *Asian J Control* 2009;11(2):144–53. <http://dx.doi.org/10.1002/asjc.090>.
- [4] Tseng AA, Notargiacomob A, Chen TP. Nanofabrication by scanning probe microscope lithography: a review. *J Vac Sci Technol* 2005;23(3):877–94.
- [5] Oliver RA. Advances in AFM for the electrical characterization of semiconductors. *Rep Progr Phys* 2008;71(7):076501.
- [6] Fleming AJ. Nanopositioning system with force feedback for high-performance tracking and vibration control. *IEEE Trans Mech* 2010;15(3):433–47.
- [7] Eielsen AA, Burger M, Gravdahl JT, Pettersen KY. PI<sup>2</sup>-controller applied to a piezoelectric nanopositioner using conditional integrators and optimal tuning. In: *Proc IFAC world congress, Milano, vol. 18; 2011*. <http://dx.doi.org/10.3182/20110828-6-IT-1002.01401>.
- [8] Abramovitch DY, Hoen S, Workman R. Semi-automatic tuning of PID gains for atomic force microscopes. In: *Proc American control conference, Seattle, WA; 2008*. p. 2684–9.
- [9] Sebastian A, Salapaka SM. Design methodologies for robust nano-positioning. *IEEE Trans Control Syst Technol* 2005;13(6):868–76. <http://dx.doi.org/10.1109/TCST.2005.854336>.
- [10] Kuiper S, Schitter G. Active damping of a piezoelectric tube scanner using self-sensing piezo actuation. *Mechatronics* 2010;20(6):656–65.
- [11] Devasia S, Eleftheriou E, Moheimani SOR. A survey of control issues in nanopositioning. *IEEE Trans Control Syst Technol* 2007;15(5):802–23.
- [12] Fanson JL, Caughey TK. Positive position feedback control for large space structures. *AIAA J* 1990;28(4):717–24.
- [13] Aphale SS, Bhikkaji B, Moheimani SOR. Minimizing scanning errors in piezoelectric stack-actuated nanopositioning platforms. *IEEE Trans Nanotechnol* 2008;7(1):79–90.
- [14] Mahmoodi SN, Ahmadian M. Modified acceleration feedback for active vibration control of aerospace structures. *Smart Mater Struct* 2010;19(6):065015.
- [15] Fleming AJ, Moheimani SOR. Sensorless vibration suppression and scan compensation for piezoelectric tube nanopositioners. *IEEE Trans Control Syst Technol* 2006;14(1):33–44.
- [16] Fleming AJ, Behrens S, Moheimani SOR. Optimization and implementation of multi-mode piezoelectric shunt damping systems. *IEEE/ASME Trans Mech* 2002;7(1):87–94.
- [17] Pota HR, Moheimani SOR, Smith M. Resonant controllers for smart structures. In: *Proc IEEE conference on decision and control, Phoenix, Arizona; 1999*. p. 631–6.
- [18] Aphale SS, Fleming AJ, Moheimani SOR. Integral resonant control of collocated smart structures. *IOP Smart Mater Struct* 2007;16:439–46. <http://dx.doi.org/10.1088/0964-1726/16/2/023>.
- [19] Fleming AJ, Aphale SS, Moheimani SOR. A new method for robust damping and tracking control of scanning probe microscope positioning stages. *IEEE Trans Nanotechnol* 2010;9(4):438–48. <http://dx.doi.org/10.1109/TNANO.2009.2032418>.
- [20] Petersen IR, Lanson A. Feedback control of negative-imaginary systems. *IEEE Control Syst* 2010;30(5):54–72. <http://dx.doi.org/10.1109/MCS.2010.937676>.
- [21] Preumont A, Dufour JP, Malekian C. Active damping by a local force feedback with piezoelectric actuators. *J Guid Control Dynam* 1992;15(2):390–5.
- [22] Preumont A, de Marneffe B, Deraemaeker A, Bossens F. The damping of a truss structure with a piezoelectric transducer. *Comput Struct* 2008;86(3–5):227–39.
- [23] Preumont A. *Vibration control of active structures*. Kluwer Academic Publishers; 2002.
- [24] Preumont A. *Mechatronics, dynamics of electromechanical and piezoelectric systems*. Dordrecht, The Netherlands: Springer; 2006.
- [25] Fleming AJ, Leang KK. Integrated strain and force feedback for high performance control of piezoelectric actuators. *Sensors Actuators A* 2010;161(1–2):256–65. <http://dx.doi.org/10.1016/j.sna.2010.04.008>.
- [26] Fleming AJ. A review of nanometer resolution position sensors: operation and performance. *Sensors Actuators A: Phys* 2013;190:106–26.
- [27] Press WH, Teukolsky SA, Vetterling WT, Flannery BP. *Numerical recipes 3rd edition: the art of scientific computing*. Cambridge University Press; 2007.
- [28] Åström KJ, Murray RM. *Feedback systems: an introduction for scientists and engineers*. Princeton University Press; 2010.